

On Far-Infrared and Submm Circular Polarization

B. T. DRAINE¹

¹*Dept. of Astrophysical Sciences, Princeton University, Princeton, NJ 08544, USA*

ABSTRACT

Interstellar dust grains are often aligned. If the grain alignment direction varies along the line of sight, the thermal emission becomes circularly-polarized. In the diffuse interstellar medium, the circular polarization at far-infrared and submm wavelengths is predicted to be very small, and probably unmeasurable. However, circular polarization may reach detectable levels in infrared dark clouds and protoplanetary disks. Measurement of circular polarization could help constrain the structure of the magnetic field in infrared dark clouds, and may shed light on the mechanisms responsible for grain alignment in protoplanetary disks.

Keywords: infrared dark clouds (787), interstellar dust (836), protoplanetary disks (1300), radiative transfer (1335)

1. INTRODUCTION

Since the discovery of starlight polarization over 70 years ago ([Hiltner 1949](#); [Hall 1949](#)), polarization has become a valuable tool for study of both the physical properties of interstellar dust and the structure of the interstellar magnetic field. Starlight polarization arises because initially unpolarized starlight becomes linearly polarized as a result of linear dichroism produced by aligned dust grains in the interstellar medium (ISM). While the physics of dust grain alignment is not yet fully understood, early investigations ([Davis & Greenstein 1951](#)) showed how spinning dust grains could become aligned with their shortest axis parallel to the magnetic field direction. Subsequent studies have identified a number of important physical processes that were initially overlooked (see the review by [Andersson et al. 2015](#)), but it remains clear that in the diffuse ISM the magnetic field establishes the direction of grain alignment, with the dust grains tending to align with their short axes parallel to the local magnetic field.

[van de Hulst \(1957\)](#) noted that if the magnetic field direction was not uniform, starlight propagating through the dusty ISM would become circularly polarized. This was further discussed by [Serkowski \(1962\)](#) and [Martin \(1972\)](#). The birefringence of the dusty ISM is responsible for converting linear polarization to circular polarization ([Serkowski 1962](#); [Martin 1972](#)). The strength of the resulting circular polarization depends on the changes in the magnetic field direction and also on the optical properties of the dust.

Circular polarization of optical light from the Crab Nebula was observed by [Martin et al. \(1972\)](#). Circular polarization of starlight was subsequently observed by [Kemp \(1972\)](#) and [Kemp & Wolstencroft \(1972\)](#); the observed degree of circular polarization, $|V|/I \lesssim 0.04\%$, was small but measurable. As had been predicted, the circular polarization V changed sign as the wavelength varied from blue

to red, passing through zero near the wavelength $\sim 0.55\mu\text{m}$ where the linear polarization peaked (Martin & Angel 1976).

Because the circular polarization depends on the change in magnetic field direction along the line of sight, it can in principle be used to study the structure of the Galactic magnetic field. Data for 36 stars near the Galactic Plane suggested a systematic bending of the field for Galactic longitudes $80^\circ \lesssim \ell < 100^\circ$ (Martin & Campbell 1976). However, these studies do not appear to have been pursued, presumably because sufficiently bright and reddened stars are sparse.

In the infrared, circular polarization has been measured for bright sources in molecular clouds (Serkowski & Rieke 1973; Lonsdale et al. 1980; Dyck & Lonsdale 1981). Measurements of linear and circular polarization were used to constrain the magnetic field structure in the Orion molecular cloud OMC-1 (Lee & Draine 1985; Aitken et al. 2006).

Circular polarization has also been observed in the infrared (K_s band) in reflection nebulae (Kwon et al. 2014, 2016, 2018), but in this case scattering is important (Fukushima et al. 2020). Scattering can convert linear to circular polarization, making interpretation dependent on the uncertain scattering geometry.

It was long understood that the nonspherical and aligned grains responsible for starlight polarization must emit far-infrared radiation which would be linearly polarized. Observations of this polarized emission now allow the magnetic field direction projected on the sky to be mapped in the general ISM (see, e.g., Planck Collaboration et al. 2015a,b; Fissel et al. 2016). Ground-based observations have provided polarization maps for high surface-brightness regions at submm frequencies (e.g., Dotson et al. 2010), and the Stratospheric Observatory for Infrared Astronomy (SOFIA) is providing polarization maps of bright regions in the far-infrared (e.g., OMC-1: Chuss et al. 2019).

ALMA observations of mm and submm emission from protoplanetary disks find that the radiation is often linearly polarized. Scattering may contribute to the polarization (Kataoka et al. 2015), but the observed polarization directions and wavelength dependence appear to indicate that a substantial fraction of the polarized radiation arises from thermal emission from aligned dust grains (Lee et al. 2021).

Previous theoretical discussions of circular polarization were mainly concerned with infrared and optical wavelengths where initially unpolarized starlight becomes polarized as a result of linear dichroism. In a medium with changing polarization direction, the resulting circular polarization is small because the linear polarization itself is typically only a few %, and the optical “phase shift” (between the two linear polarization modes) produced by the aligned medium is likewise small. At far-infrared wavelengths, however, the radiation is already substantially polarized when it is emitted, with linear polarizations of 20% or more under favorable conditions (Planck Collaboration et al. 2020). While absorption optical depths tend to be small at long wavelengths, the optical properties of the dust are such that phase shift cross sections at submillimeter wavelengths can be much larger than absorption cross sections, raising the possibility that a medium with changing alignment direction might exhibit measurable levels of circular polarization at far-infrared or submm wavelengths.

The present paper discusses polarized radiative transfer in a medium with partially aligned nonspherical grains, including both absorption and thermal emission. We estimate the expected degree of circular polarization for emission from molecular clouds and protoplanetary disks. For nearby molecular clouds, the far-infrared circular polarization is very small, and probably unobservable. The circular polarization is predicted to be larger for so-called infrared dark clouds (IRDCs), although it is still small. For protoplanetary disks the circular polarization may be measurable, but will depend on how the direction of grain alignment changes in the disk.

The paper is organized as follows. The equations describing propagation of partially-polarized radiation are presented in Section 2, and the optics of partially-aligned dust mixtures are summarized in Section 3. Section 4 estimates the circularly polarized emission from molecular clouds, including IRDCs. Section 5 discusses the alignment of solid particles in stratified protoplanetary

disks resembling HL Tau. If the grain alignment is due to dust-gas streaming, the emission may be circularly-polarized. The results are discussed in Section 6, and summarized in Section 7.

2. POLARIZED RADIATIVE TRANSFER

2.1. *Refractive Index of a Dusty Medium*

Aligned dust grains result in linear dichroism – the attenuation coefficient depends on the linear polarization of the radiation. Linear dichroism is responsible for the polarization of starlight – initially unpolarized light from a star becomes linearly polarized as the result of polarization-dependent attenuation by aligned dust grains.

We adopt the convention that the electric field $E \propto \text{Re}[e^{imkz - i\omega t}]$ for a wave propagating in the $+\hat{\mathbf{z}}$ direction, where $k \equiv \omega/c = 2\pi/\lambda$ is the wave vector *in vacuo*, and $m(\omega)$ is the complex refractive index of the dusty medium. For radiation polarized with $\mathbf{E} \parallel \hat{\mathbf{e}}_j$, the complex refractive index is

$$m_j \equiv 1 + m'_j + im''_j \quad . \quad (1)$$

The real part m'_j describes retardation of the wave, relative to propagation *in vacuo*. The phase delay ϕ varies as

$$\frac{d\phi_j}{dz} = \frac{2\pi}{\lambda} m'_j = n_d C_{\text{pha},j} \quad , \quad (2)$$

where n_d is the number density of dust grains, and $C_{\text{pha},j}$ is the “phase shift” cross section of a grain. The imaginary part m''_j describes attenuation of the energy flux F :

$$\frac{d \ln F}{dz} = -\frac{4\pi}{\lambda} m''_j = -n_d C_{\text{ext},j} \quad , \quad (3)$$

where $C_{\text{ext},j}$ is the extinction cross section.

2.2. *Transfer Equations for the Stokes Parameters*

Consider a beam of radiation characterized by the usual Stokes vector $\mathbf{S} \equiv (I, Q, U, V)$. The equations describing transfer of radiation through a dichroic and birefringent medium with changing magnetic field direction have been discussed by [Serkowski \(1962\)](#) and [Martin \(1974\)](#).¹ The discussions have assumed that the aligned grains polarize the light by preferential attenuation of one of the polarization modes, with circular polarization then arising from differences in propagation speed of the linearly polarized modes.

For submicron particles, scattering is negligible at far-infrared wavelengths, because the grain is small compared to the wavelength. However, the grains are themselves able to radiate, and aligned grains will emit polarized radiation.

Let the direction of the static magnetic field \mathbf{B}_0 be

$$\hat{\mathbf{b}} \equiv \frac{\mathbf{B}_0}{|\mathbf{B}_0|} = (\hat{\mathbf{n}} \cos \Psi + \hat{\mathbf{e}} \sin \Psi) \sin \gamma + \hat{\mathbf{z}} \cos \gamma \quad (4)$$

where $\hat{\mathbf{n}}$ and $\hat{\mathbf{e}}$ are unit vectors in the North and East directions, $\hat{\mathbf{z}} = \hat{\mathbf{n}} \times \hat{\mathbf{e}}$ is the direction of propagation, and $\sin \gamma = 1$ if $\hat{\mathbf{b}}$ is in the plane of the sky.

Let $\hat{\mathbf{x}}$ and $\hat{\mathbf{y}}$ be orthonormal vectors in the plane of the sky, with $\hat{\mathbf{x}}$ parallel to the projection of \mathbf{B}_0 on the plane of the sky (see Figure 1):

$$\hat{\mathbf{x}} = \hat{\mathbf{n}} \cos \Psi + \hat{\mathbf{e}} \sin \Psi \quad (5)$$

$$\hat{\mathbf{y}} = -\hat{\mathbf{n}} \sin \Psi + \hat{\mathbf{e}} \cos \Psi \quad . \quad (6)$$

¹ Our axes $\hat{\mathbf{x}}$ and $\hat{\mathbf{y}}$ correspond, respectively, to axes 2 and 1 in [Martin \(1974\)](#).

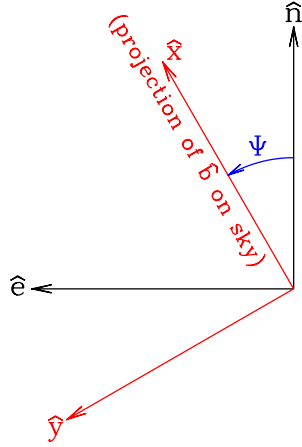


Figure 1. Angle Ψ , and directions $\hat{\mathbf{x}}$, $\hat{\mathbf{y}}$.

If the dust grains are partially aligned with their short axes tending to be parallel to \mathbf{B}_0 , we expect $C_{\text{ext},y} > C_{\text{ext},x}$. At long wavelengths ($\lambda \gg 10\mu\text{m}$) we also expect $C_{\text{pha},y} > C_{\text{pha},x}$. We assume that the dust grains themselves have no overall chirality, hence circular dichroism and circular birefringence can be neglected so long as the response of the magnetized plasma is negligible, which is generally the case for $\nu \gtrsim 30\text{ GHz}$.

Following the notation of [Martin \(1974\)](#), define

$$\delta \equiv n_d \frac{(C_{\text{ext},y} + C_{\text{ext},x})}{2} = \frac{2\pi}{\lambda} (m''_x + m''_y) \quad (7)$$

$$\Delta\sigma \equiv n_d \frac{(C_{\text{ext},y} - C_{\text{ext},x})}{2} = \frac{2\pi}{\lambda} (m''_y - m''_x) \quad (8)$$

$$\Delta\epsilon \equiv n_d \frac{(C_{\text{pha},y} - C_{\text{pha},x})}{2} = \frac{2\pi}{\lambda} \frac{(m'_y - m'_x)}{2}. \quad (9)$$

If scattering is neglected, the propagation of the Stokes parameters is given by²

$$\frac{d}{dz} \begin{pmatrix} I \\ Q \\ U \\ V \end{pmatrix} = \begin{pmatrix} -\delta & \Delta\sigma \cos 2\Psi & \Delta\sigma \sin 2\Psi & 0 \\ \Delta\sigma \cos 2\Psi & -\delta & 0 & \Delta\epsilon \sin 2\Psi \\ \Delta\sigma \sin 2\Psi & 0 & -\delta & -\Delta\epsilon \cos 2\Psi \\ 0 & -\Delta\epsilon \sin 2\Psi & \Delta\epsilon \cos 2\Psi & -\delta \end{pmatrix} \begin{pmatrix} I - B(T_d) \\ Q \\ U \\ V \end{pmatrix}, \quad (10)$$

where $B(T_d)$ is the intensity of blackbody radiation for dust temperature T_d . Eq. (10) differs from [Martin \(1974\)](#) only by replacement of I by $(I - B)$ on the right-hand side to allow for thermal emission (see also [Reissl et al. 2016](#)). It is apparent that Eq. (10) is consistent with thermal equilibrium blackbody radiation, with $d\mathbf{S}/dz = 0$ for $\mathbf{S} = (B, 0, 0, 0)$.

3. OPTICAL PROPERTIES OF THE DUST

We now assume that the grains can be approximated by spheroids. [Draine & Hensley \(2021a\)](#) found that observations of starlight polarization and far-infrared polarization appear to be consistent with

² Eq. (10) conforms to the IEEE and IAU conventions for the Stokes parameters ([Hamaker & Bregman 1996](#)): $Q > 0$ for \mathbf{E} along the N-S direction, $U > 0$ for \mathbf{E} along the NE-SW direction, $V > 0$ for “right-handed” circular polarization (\mathbf{E} rotating in the counterclockwise direction as viewed on the sky).

dust with oblate spheroidal shapes, with axial ratio $b/a \approx 1.6$ providing a good fit to observations. Observations of the diffuse ISM are consistent with

$$\frac{\delta}{n_{\text{H}}} = \frac{\tau}{N_{\text{H}}} \approx 6.5 \times 10^{-27} \left(\frac{\lambda}{\text{mm}} \right)^{-1.8} \text{cm}^2 \text{H}^{-1} \quad (11)$$

for $100\mu\text{m} \lesssim \lambda \lesssim 1\text{cm}$ (Hensley & Draine 2021; Draine & Hensley 2021b).

Let $\hat{\mathbf{b}}$ be a “special” direction in space for grain alignment: the short axis $\hat{\mathbf{a}}_1$ of the grain may be preferentially aligned either parallel or perpendicular to $\hat{\mathbf{b}}$. For grains in the diffuse ISM, $\hat{\mathbf{b}}$ is the magnetic field direction, and the short axis $\hat{\mathbf{a}}_1$ tends to be parallel to $\hat{\mathbf{b}}$. In protostellar disks, however, other alignment mechanisms may operate, and $\hat{\mathbf{b}}$ may not be parallel to the magnetic field.

We approximate the grains by oblate spheroids, spinning with short axis $\hat{\mathbf{a}}_1$ parallel to the angular momentum \mathbf{J} . For oblate spheroids, the fractional alignment is defined to be

$$f_{\text{align}} \equiv \frac{3}{2} \langle (\hat{\mathbf{a}}_1 \cdot \hat{\mathbf{b}})^2 \rangle - \frac{1}{2} \quad , \quad (12)$$

where $\langle \dots \rangle$ denotes averaging over the grain population. If $\mathbf{J} \parallel \hat{\mathbf{b}}$, then $f_{\text{align}} \rightarrow 1$; if \mathbf{J} is randomly-oriented, then $f_{\text{align}} = 0$; if $\mathbf{J} \perp \hat{\mathbf{b}}$, then $f_{\text{align}} \rightarrow -\frac{1}{2}$.

The “modified picket fence approximation” (Draine & Hensley 2021a) relates δ , $\Delta\sigma$, and $\Delta\epsilon$ to f_{align} and the angle γ :

$$\delta = n_d \left[\frac{C_{\text{abs},a} + 2C_{\text{abs},b}}{3} + f_{\text{align}} \left(\cos^2 \gamma - \frac{1}{3} \right) \frac{(C_{\text{abs},b} - C_{\text{abs},a})}{2} \right] \quad (13)$$

$$\Delta\sigma = n_d f_{\text{align}} \sin^2 \gamma \frac{(C_{\text{abs},b} - C_{\text{abs},a})}{2} \quad (14)$$

$$\Delta\epsilon = n_d f_{\text{align}} \sin^2 \gamma \frac{(C_{\text{pha},b} - C_{\text{pha},a})}{2} \quad . \quad (15)$$

In the Rayleigh limit (grain radius $a \ll \lambda$) we have (Draine & Lee 1984)

$$C_{\text{abs},j} = \frac{2\pi V}{\lambda} \frac{\epsilon_2}{|1 + (\epsilon - 1)L_j|^2} \quad (16)$$

$$C_{\text{pha},j} = \frac{\pi V}{\lambda} \frac{\{(\epsilon_1 - 1)[1 + L_j(\epsilon_1 - 1)] + \epsilon_2^2 L_j\}}{|1 + (\epsilon - 1)L_j|^2} \quad , \quad (17)$$

where $\epsilon(\lambda) \equiv \epsilon_1 + i\epsilon_2$ is the complex dielectric function of the grain material, and L_a and $L_b = (1 - L_a)/2$ are dimensionless “shape factors” (van de Hulst 1957; Bohren & Huffman 1983) that depend on the axial ratio of the spheroid. Draine & Hensley (2021b) have estimated $\epsilon(\lambda)$ of astrodust for different assumed axial ratios.

Figure 2 shows the dimensionless ratios $\Delta\sigma/\delta$ and $\Delta\epsilon/\delta$ for oblate astrodust spheroids with porosity $\mathcal{P} = 0.2$, $b/a = 1.6$ ($L_a = 0.464$, $L_b = 0.268$) and $f_{\text{align}} = 0.5$, for the case where the magnetic field is in the plane of the sky ($\sin \gamma = 1$). The relatively high opacity that enables “astrodust” to reproduce the observed far-infrared emission and polarization also implies that ϵ_1 has to be fairly large at long wavelengths (Draine & Hensley 2021b). This causes $\Delta\epsilon/\delta$ to be relatively large, as seen in Figure 2. For $\lambda \gtrsim 70\mu\text{m}$, oblate astrodust grains with $b/a = 1.6$ have

$$\frac{\Delta\sigma}{\delta} \approx 0.38 f_{\text{align}} \sin^2 \gamma \quad (18)$$

$$\frac{\Delta\epsilon}{\delta} \approx 9.0 \left(\frac{\lambda}{\text{mm}} \right)^{0.7} f_{\text{align}} \sin^2 \gamma \quad . \quad (19)$$

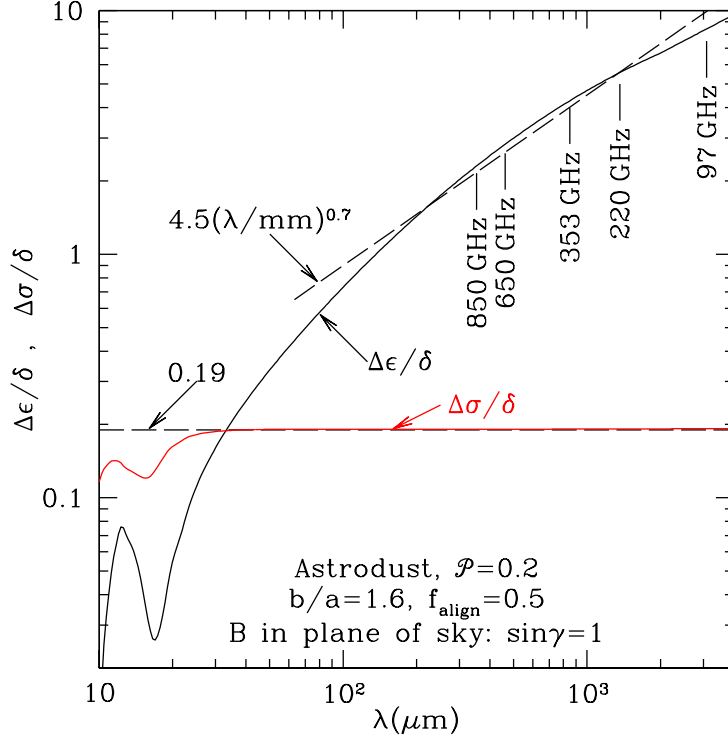


Figure 2. The ratios $\Delta\sigma/\delta$ and $\Delta\epsilon/\delta$ for oblate astrodust spheroids with porosity $\mathcal{P} = 0.2$, axial ratio $b/a = 1.6$, alignment fraction $f_{\text{align}} = 0.5$, and $\sin^2 \gamma = 1$ (magnetic field in the plane of the sky). The power-law approximation (19) for $\Delta\epsilon/\delta$ is also shown.

Eq. (18) and (19) neglect the weak dependence of δ on f_{align} and γ (see Eq. 13). Eqs. (18) and ((19) are shown in Figure 2 for $f_{\text{align}} \sin^2 \gamma = 0.5$.

4. CIRCULAR POLARIZATION FROM INTERSTELLAR CLOUDS

4.1. Grain Alignment

A spinning grain develops a magnetic moment from the Barnett effect (if it has unpaired electrons) and the Rowland effect (if it has a net charge). For submicron grains, the resulting net magnetic moment is large enough that the Larmor precession period in the local interstellar magnetic field is short compared to the timescales for other mechanisms to change the direction of the grain's angular momentum \mathbf{J} . The rapid precession of \mathbf{J} around the local magnetic field \mathbf{B}_0 and the resulting averaging of grain optical properties establishes \mathbf{B}_0 as the special direction for grain alignment – grains will be aligned with their short axis preferentially oriented either parallel or perpendicular to \mathbf{B}_0 .

Paramagnetic dissipation, radiative torques, or systematic streaming of the grains relative to the gas will determine whether the grains align with their short axes preferentially parallel or perpendicular to \mathbf{B}_0 . Although the details of the physics of grain alignment are not yet fully understood, it is now clear that grains in diffuse and translucent clouds tend to align with short axes $\hat{\mathbf{a}}_1$ tending to be parallel to \mathbf{B}_0 , i.e., with $f_{\text{align}} > 0$ (see Eq. 12).

If the dust grains are modeled by oblate spheroids with axial ratio $b/a = 1.6$, a mass-weighted alignment fraction $f_{\text{align}} \approx 0.5$ can reproduce the highest observed levels of polarization of both starlight and far-infrared emission from dust in diffuse clouds (including diffuse molecular clouds) (Draine & Hensley 2021a).

In dark clouds, the fractional polarization of the thermal emission is generally lower than in diffuse clouds. The lower fractional polarization may indicate lower values of f_{align} within dark clouds, but it could also result from a nonuniform magnetic field in the cloud, with the overall linear polarization fraction reduced by beam-averaging over regions with different polarization directions.

If the reduced values of linear polarization are due to systematic changes in magnetic field direction along the line-of-sight, the emission from the cloud could become partly circularly-polarized. We now estimate what levels of circular polarization might be present.

4.2. Nearby Molecular Clouds

Planck has observed linearly polarized emission from many molecular clouds. To estimate the levels of circular polarization that might be present, we consider one illustrative example, in the “RCrA-Tail” region in the R Corona Australis molecular cloud (see Fig. 11 in [Planck Collaboration et al. 2015a](#)). The polarized emission in this region has a number of local maxima. One of the polarized flux maxima coincides with a total emission peak near $(\ell, b) \approx (-0.9^\circ, -18.7^\circ)$, with total intensity $I(353 \text{ GHz}) \approx 4 \text{ MJy sr}^{-1}$ and linear polarization fraction $p \approx 2.5\%$.

For an assumed dust temperature $T_d \approx 15 \text{ K}$, the observed intensity $I(353 \text{ GHz}) = 4 \text{ MJy sr}^{-1}$ implies $\tau(353 \text{ GHz}) \approx 1.3 \times 10^{-4}$. For diffuse ISM dust (see, e.g. [Hensley & Draine 2021](#)), this would correspond to $A_V \approx 5 \text{ mag}$.

For simple assumptions about the angle Ψ characterizing the projection of the magnetic field on the sky, we can obtain approximate analytic solutions to the radiative transfer equations (10), valid for $\tau \ll 1$ (see Appendix A). Define $d\tau' \equiv \delta dz$. Suppose that T_d , $(\Delta\sigma/\delta)$, and $(\Delta\epsilon/\delta)$ are constant, and assume that the magnetic field direction has a smooth twist along the line of sight, with Ψ varying linearly with τ' as τ' varies from 0 to τ :

$$\Psi = \Psi_0 + \alpha\tau' \quad , \quad \alpha \equiv \frac{\Delta\Psi}{\tau} \quad . \quad (20)$$

For $\tau \ll 1$, the linear and circular polarization fractions are then (see Appendix A)

$$p \approx \left(\frac{\Delta\sigma}{\delta} \right) \frac{[1 - \cos(2\Delta\Psi)]^{1/2}}{\Delta\Psi} \quad (21)$$

$$\frac{V}{I} \approx \left(\frac{\Delta\sigma}{\delta} \right) \left(\frac{\Delta\epsilon}{\delta} \right) \frac{\tau}{2\Delta\Psi} \left[1 - \frac{\sin(2\Delta\Psi)}{2\Delta\Psi} \right] \quad . \quad (22)$$

Eq. (21–22) are for the special case of an isothermal medium with a uniform twist in the alignment direction.

If we assume diffuse cloud dust properties (Eq. 18, 19) but with $f_{\text{align}} \sin^2 \gamma = 0.075$ and a twist angle $\Delta\Psi = 90^\circ$, we can reproduce the observed polarization $p \approx 2.5\%$ in the RCrA-Tail region. With these parameters, Eq. (22) predicts circular polarization $V/I \approx 7 \times 10^{-7} (\lambda/850 \mu\text{m})^{-1.1}$, far below current sensitivity limits. It is clear that measurable levels of circular polarization in the far-infrared will require much larger optical depths τ .

4.3. Infrared Dark Clouds

Typical giant molecular clouds (GMCs), such as the Orion Molecular Cloud, have mass surface densities resulting in $A_V \approx 10 \text{ mag}$ of extinction, and are therefore referred to as “dark clouds”. However, in the inner Galaxy, a number of clouds have been observed that appear to be “dark” (i.e., opaque) even in the mid-infrared. These “infrared dark clouds” (IRDCs) have dust masses per area an order of magnitude larger than “typical” giant molecular clouds. Because of the much larger extinction in IRDCs, the circular polarization may be much larger than in normal GMCs.

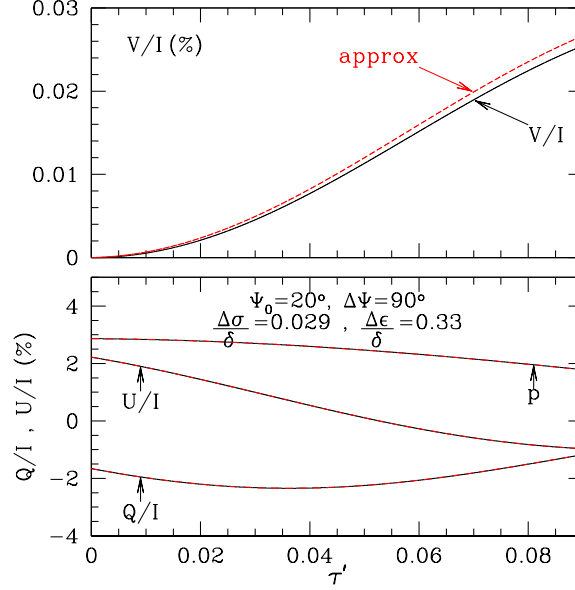


Figure 3. Stokes parameters for radiation from a dust slab resembling the Brick IRDC, as a function of the optical depth τ' along the path. The properties of astrodust at 850 GHz ($350\mu\text{m}$) are assumed, with $f_{\text{align}} \sin^2 \gamma = 0.075$, and a field rotation $\Delta\Psi = 90^\circ$. Black curves: numerical results. Red curves: analytic approximations (A2–A6).

The “Brick” (G0.253+0.016) is a well-studied IRDC (Carey et al. 1998; Longmore et al. 2012). With an estimated mass $M > 10^5 M_\odot$ and high estimated density ($n_{\text{H}} > 10^4 \text{ cm}^{-3}$), the Brick appears to be forming stars (Marsh et al. 2016; Walker et al. 2021), although with no signs of high-mass star formation. It has been mapped at $70 - 500\mu\text{m}$ by Herschel Space Observatory (Molinari et al. 2016) and at 220 GHz by ACT (Guan et al. 2021). Polarimetric maps have been made at 220 GHz by ACT, and at 850 GHz by the CSO (Dotson et al. 2010).

The Northeastern region at $(\ell, b) = (16', 2')$ has $I(600 \text{ GHz}) \approx 5000 \text{ MJy sr}^{-1}$ (Molinari et al. 2016) and $I(220 \text{ GHz}) \approx 90 \text{ MJy sr}^{-1}$ (Guan et al. 2021). For an assumed dust temperature $T_d \approx 20 \text{ K}$, this indicates optical depths $\tau(600 \text{ GHz}) \approx 0.05$, $\tau(220 \text{ GHz}) \approx 0.005$. Astrodust would then have $\tau(850 \text{ GHz}) \approx 0.09$, and $\tau(353 \text{ GHz}) \approx 0.014$ – about 100 times larger than in the R CrA molecular cloud.

The fractional polarization is expected to be approximately independent of frequency in the submm. At 220 GHz, (Guan et al. 2021) report a linear polarization of 1.8% at 220 GHz for the Northeastern end of the cloud, $(\ell, b) \approx (16', 2.5')$ (Yilun Guan 2021, private communication). The CSO polarimetry suggests a similar fractional polarization at 850 GHz.

While this fractional polarization is relatively small compared to the highest values ($\sim 20\%$) observed by Planck in diffuse clouds, it is still appreciable, requiring significant grain alignment in a substantial fraction of the cloud volume (i.e., not just in the surface layers of the IRDC). The inferred average magnetic field direction $\Psi \approx 20^\circ$ (Guan et al. 2021) differs by $\sim 60^\circ$ from the $\Psi \approx 80^\circ$ field direction indicated by the 220 GHz polarization outside the cloud, demonstrating that the magnetic field in this region is far from uniform.

As a simple example, we suppose, as we did for the RCrA-Tail region above, that the projected field rotates by $\Delta\Psi = 90^\circ$ from the far side of the “Brick” to the near side.

We calculate the circular polarization at 850 GHz ($350\mu\text{m}$) for the estimated total optical depth $\tau(850 \text{ GHz}) = 0.09$ of the Brick. We use the estimated properties of astrodust in the diffuse ISM, with $f_{\text{align}} \sin^2 \gamma = 0.075$ to approximately reproduce the $\sim 1.8\%$ polarization observed for the Brick.

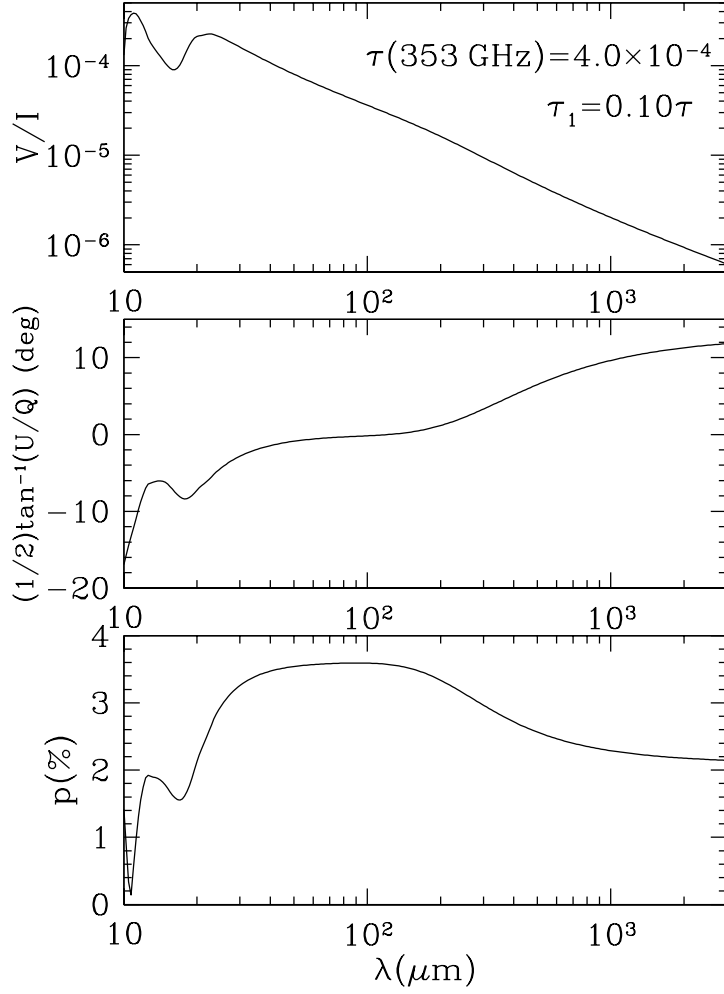


Figure 4. Polarization of dust continuum from a molecular cloud with a PDR on the far side. The magnetic field in the cold cloud is assumed to have a systematic twist along the line of sight, with a twist angle $\Delta\Psi = 60^\circ$. The dust is assumed to be partially aligned, with $f_{\text{align}} \sin^2 \gamma = 0.1$ for the warm dust ($T_1 = 80$ K) in the PDR, and $f_{\text{align}} \sin^2 \gamma = 0.05$ for the cold dust ($T_2 = 15$ K) in the rest of the cloud.

Figure 2 shows the polarization state of the radiation as it propagates through the cloud from $\tau' = 0$ to $\tau' = \tau$. The fractional polarization p starts off at $\sim 2.9\%$, dropping to $\sim 1.8\%$ at $\tau' = \tau$ as the result of the assumed magnetic field twist of $\Delta\Psi = 90^\circ$.

The resulting 850 GHz circular polarization V/I is small, only $\sim 0.025\%$. Measuring such low levels of circular polarization will be challenging. For $\Delta\epsilon/\delta \propto \lambda^{0.7}$ (see Figure 2) and the absorption coefficient $\delta \propto \lambda^{-1.8}$ (see Eq. 11), the circular polarization from an IRDC is expected to vary as $V/I \propto \lambda^{-1.1}$. For the adopted parameters ($\Delta\Psi = 90^\circ$, $\tau(850 \text{ GHz}) = 0.09$, $f_{\text{align}} \sin^2 \gamma = 0.075$), the Brick would have

$$\frac{V}{I} \approx 0.025\% \left(\frac{350 \mu\text{m}}{\lambda} \right)^{1.1} \quad (23)$$

for $70 \mu\text{m} \lesssim \lambda \lesssim 1 \text{ cm}$. While much larger than for normal GMCs, this estimate for the circularly-polarized emission from the Brick is small, and measuring it will be challenging.

4.4. PDR Seen Through a Molecular Cloud

The warm dust surrounding an embedded HII region may allow measurement of circular polarization at wavelengths as short as $\sim 20\mu\text{m}$. We consider a cloud with optical depth $\tau(353\text{ GHz}) = 4 \times 10^{-4}$, somewhat greater than the R Corona Australis cloud example considered in Section 4.2, but small compared to the Brick.

The far edge of the cloud is assumed to contain warm dust in a photodissociation region (PDR) with optical depth $\tau_1(\lambda)$. The PDR is assumed to contribute 10% of the total column density through the molecular cloud, with dust heated to $T_1 = 80\text{ K}$. The dust in the rest of the molecular cloud is cold, $T_2 = 15\text{ K}$.

We assume the dust in the PDR to be moderately aligned, with $f_{\text{align}} \sin^2 \gamma = 0.1$, whereas for the dust in the rest of the molecular cloud we take $f_{\text{align}} \sin^2 \gamma = 0.05$.

Using the analytic approximation for the “two-zone” model in Appendix B, we find the fractional linear polarization p and circular polarization V/I shown in Figure 4. At $\lambda \lesssim 100\mu\text{m}$, the polarization is the combination of polarized emission from the warm dust in the PDR and dichroic absorption by the cool dust. At longer wavelengths, $\lambda > 300\mu\text{m}$, dichroic absorption is minimal, and we see the sum of the polarized emission from the warm and cool regions. The polarization angle rotates as the ratio of warm emission to cool emission drops with increasing wavelength. The features at $10 < \lambda < 30\mu\text{m}$ arise from the strong silicate absorption bands at 10 and $18\mu\text{m}$.

The circular polarization reaches $V/I = 0.02\%$ at $\lambda = 20\mu\text{m}$ but declines as $\sim \lambda^{-1.1}$ at longer wavelengths.

5. CIRCULAR POLARIZATION FROM PROTOPLANETARY DISKS

Protoplanetary disks can have dust surface densities well in excess of IRDCs, raising the possibility that τ may be large enough to generate measurable circular polarization if the grains are locally aligned *and* the alignment direction varies along the optical path.

5.1. Grain Alignment in Protoplanetary Disks

Gas densities in protoplanetary disks exceed interstellar gas densities by many orders of magnitude. The observed thermal emission spectra from young protoplanetary disks appear to require that most of the solid material be in particles with sizes that may be as large as $\sim\text{mm}$ (Beckwith & Sargent 1991; Natta & Testi 2004; Draine 2006), orders of magnitude larger than the submicron grains in the diffuse ISM.

The physics of grain alignment in protoplanetary disks differs substantially from the processes in the diffuse ISM. One important difference from interstellar clouds is that in protoplanetary disks the Larmor precession period for the grain sizes of interest is *long* compared to the time for the grain to undergo collisions with a mass of gas atoms equal to the grain mass (Yang 2021). With Larmor precession no longer important, the magnetic field no longer determines the preferred direction for grain alignment. Instead, the “special” direction may be either the local direction of gas-grain streaming – in which case, $\hat{\mathbf{b}} \parallel \mathbf{v}_{\text{drift}}$ – or perhaps the direction of anisotropy in the radiation field – in which case, $\hat{\mathbf{b}} \parallel \mathbf{r}$. Whether grains will tend to align with short axes $\hat{\mathbf{a}}_1$ parallel or perpendicular to $\hat{\mathbf{b}}$ (i.e., $f_{\text{align}} > 0$ or $f_{\text{align}} < 0$) is a separate question.

5.1.1. Alignment by Radiative Torques?

Radiative torques resulting from outward-directed radiation provide one possible mechanism for grain alignment. Starlight torques have been found to be very important for both spinup and alignment of interstellar grains (Draine & Weingartner 1996, 1997; Weingartner & Draine 2003; Lazarian & Hoang 2007a). With mm-sized grains, both stellar radiation and infrared emission from the disk may be capable of exerting systematic torques large enough to affect the spin of the grain. However, the radiation pressure $\sim L_*/4\pi R^2 c \approx 5 \times 10^{-9} (L_*/L_\odot) (100\text{ AU}/R)^2 \text{ erg cm}^{-3}$ is small compared to

the gas pressure $\sim 8 \times 10^{-5} (n_{\text{H}}/10^{10} \text{ cm}^{-3}) (T/100 \text{ K}) \text{ erg cm}^{-3}$. If the grain streaming velocity exceeds $\sim 10^{-4} c_s$, where c_s is the sound speed, systematic torques exerted by gas atoms may dominate radiative torques. Studies of realistic grain geometries are needed to clarify the relative importance of gaseous and radiative torques.

5.1.2. Alignment by Grain Drift?

The differential motion of dust and gas in three-dimensional disks has been discussed by Takeuchi & Lin (2002). Grains well above or below the midplane will sediment toward the midplane, with $\mathbf{v}_{\text{drift}} \parallel \mathbf{z}_{\text{disk}}$, where z_{disk} is height above the midplane. Dust grains close to the midplane will be in near-Keplerian orbits, but will experience a “headwind”, with $\mathbf{v}_{\text{drift}} \parallel \hat{\phi}$. Vertical and azimuthal drift velocities will in general differ, with different dependences on grain size and radial distance from the protostar.

Gold (1952) proposed grain drift relative to the gas as an alignment mechanism. For hypersonic motion, Gold concluded that needle-shaped particles would tend to align with their short axes perpendicular to $\mathbf{v}_{\text{drift}}$. Purcell (1969) analyzed spheroidal shapes, finding that significant alignment requires hypersonic gas-grain velocities if the grains are treated as rigid bodies. The degree of grain alignment of spheroidal grains is increased when dissipative processes within the grain are included (Lazarian 1994), but the degree of alignment is small unless the streaming is supersonic.

Lazarian & Hoang (2007b) discussed mechanical alignment of subsonically-drifting grains with “helicity”, arguing that helical grains would preferentially acquire angular momentum parallel or antiparallel to $\mathbf{v}_{\text{drift}}$; internal dissipation would then cause the short axis to tend to be *parallel* to $\mathbf{v}_{\text{drift}}$. Lazarian & Hoang (2007b) based their analysis on a simple geometric model of a spheroidal grain with a single projecting panel. More realistic irregular geometries have been considered by Das & Weingartner (2016) and Hoang et al. (2018). However, these studies all assumed Larmor precession to be rapid compared to the gas-drag time, and are therefore not directly applicable to protoplanetary disks.

It appears possible that, averaged over the ensemble of irregular grain shapes, the net effect of gas-grain streaming in protoplanetary disks may be (1) suprathermal angular momenta tending to be perpendicular to $\mathbf{v}_{\text{drift}}$, and (2) tendency of grains to align with short axes perpendicular to $\mathbf{v}_{\text{drift}}$. Below, we consider the consequences of this conjecture.

5.2. The HL Tau Disk as an Example

ALMA has observed a number of protoplanetary disks (e.g., Andrews et al. 2018). HL Tau remains one of the best-observed cases: it is nearby ($\sim 140 \text{ pc}$), bright, and moderately inclined ($i \approx 45^\circ$). The optical depth in the disk is large, with beam-averaged $\tau(3.1 \text{ mm}) \approx 0.13$ at $R \approx 100 \text{ AU}$.³ Given that the dust is visibly concentrated in rings, and the possibility that there may be additional unresolved substructure, the actual optical depth of the emitting regions at 100 AU is likely to be larger.

The polarization in HL Tau has been mapped by ALMA at $870 \mu\text{m}$, 1.3 mm, and 3.1 mm (Kataoka et al. 2017; Stephens et al. 2017). The observed polarization patterns show considerable variation from one frequency to another, complicating interpretation. Both intrinsic polarization from aligned grains and polarization resulting from scattering appear to be contributing to the overall polarization. Mori & Kataoka (2021) argue that polarized emission makes a significant contribution to the polarization, at least at 3.1 mm.

The 3.1 mm polarization pattern is generally azimuthal (Stephens et al. 2017). If due to polarized emission, this would require that the radiating dust grains have short axes preferentially oriented in the radial direction. The alignment mechanism is unclear.

³ At $R \approx 100 \text{ AU}$, $I_\nu(3.1 \text{ mm}) \approx 1.1 \times 10^3 \text{ MJy sr}^{-1}$ (Kataoka et al. 2017; Stephens et al. 2017), implying $\tau \approx 0.13$ if the dust temperature $T_d \approx 30 \text{ K}$ (Okuzumi & Tazaki 2019).

Table 1. A Stratified Disk Example^a

Parameter	lower layer $j = 1$	midplane $j = 2$	upper layer $j = 3$
τ_j	0.05	0.2	0.05
$B(T_{d,j})/B(T_{d,2})$	2	1	2
$\sin \gamma$	$\cos \theta_i$	$1 \rightarrow \sin \theta_i$	$\cos \theta_i$
Ψ_j	0	$0 \rightarrow 180^\circ$	180°
f_{align}	-0.2	-0.2	-0.2
$(\Delta\sigma/\delta)_j$	$0.38f_{\text{align}} \sin^2 \gamma$	$0.38f_{\text{align}} \sin^2 \gamma$	$0.38f_{\text{align}} \sin^2 \gamma$
$(\Delta\epsilon/\delta)_j$	$19f_{\text{align}} \sin^2 \gamma$	$19f_{\text{align}} \sin^2 \gamma$	$19f_{\text{align}} \sin^2 \gamma$

For $\lambda = 3.1$ mm.

Kataoka et al. (2019) favor radiative torques, with the grain's short axis assumed to be *parallel* to the radiative flux, in the radial direction. This would be consistent with the observation that the linear polarization tends to be in the azimuthal direction. If radiative torques are responsible for grain alignment in protoplanetary disks, then we do not expect the thermal emission from the disk to be circularly polarized, because the grains in the upper and lower layers of the disk will tend to have the same alignment direction as the grains near the midplane. If there is no change in the direction of the grain alignment along a ray, there will be no circular polarization.

Here we instead suppose that grain alignment is dominated by gas-grain streaming due to systematic motion of the dust grains relative to the local gas. If we define $\hat{\mathbf{b}} \parallel \mathbf{v}_{\text{drift}}$ we can apply the discussion above. As discussed above, we conjecture that the irregular grains align with short axes tending to be *perpendicular* to $\mathbf{v}_{\text{drift}}$, thus $f_{\text{align}} < 0$.

As before, let γ be the angle between the line-of-sight and $\hat{\mathbf{b}}$, and let Ψ be the angle (relative to north) of the projection of $\hat{\mathbf{b}}$ on the plane of the sky. For illustration, we take the disk to have the major axis in the E-W direction (see Figure 5), with inclination i . Thus vertical drifts correspond to $\Psi = 0$ and 180° . The treatment of radiative transfer developed above for magnetized clouds can be reapplied to protoplanetary disks – the only difference is that if the grains align with their short axis tending to be perpendicular to $\mathbf{v}_{\text{drift}}$ then $f_{\text{align}} < 0$, implying $\Delta\sigma < 0$ and $\Delta\epsilon < 0$.

The direction and magnitude of $\mathbf{v}_{\text{drift}}$ will vary with height in the disk. $\mathbf{v}_{\text{drift}}$ may be approximately normal to the disk plane for grains that are falling toward the midplane, whereas $\mathbf{v}_{\text{drift}}$ will be azimuthal for grains near the midplane, with Keplerian rotation causing them to move faster than the pressure-supported gas disk. Thus, grain orientations may vary both vertically and azimuthally. With Ψ varying along a ray, the emerging radiation may be partially circularly-polarized.

The observed linear polarization of a few percent suggests that $|\Delta\sigma/\delta| \approx$ a few %.

We do not expect Ψ to vary linearly with τ as in Eq. (A1): the variation of Ψ along the ray will depend on the varying grain dynamics along the ray. To investigate what levels of circular polarization might be present, we consider an idealized model with three dust layers: layer 2 is the dust near the midplane, and layers 1 and 3 contain the dust below and above the midplane. Conditions in layers 1 and 3 are assumed to be identical. Let τ_j be the optical depth through layer j . Assume that $\hat{\mathbf{b}}$ is normal to the disk in layers 1 and 3, and azimuthal in layer 2 (see Figure 5). Thus $\Psi_1 = \Psi_3$. For

small values of τ_1 , τ_2 , and τ_3 we can approximate the radiative transfer (see Appendix C):

$$I_1 = B_1 \tau_1 \left(1 - \frac{1}{2} \tau_1\right) e^{-\tau_2 - \tau_3} \quad (24)$$

$$I_2 = B_2 \tau_2 \left(1 - \frac{1}{2} \tau_2\right) e^{-\tau_3} \quad (25)$$

$$I_3 = B_3 \tau_3 \left(1 - \frac{1}{2} \tau_3\right) \quad (26)$$

$$I \approx I_1 + I_2 + I_3 \quad (27)$$

$$Q \approx - \left(\frac{\Delta\sigma}{\delta}\right)_3 \cos(2\Psi_3) [I_1 + I_3 - \tau_3(I_1 + I_2)] - \left(\frac{\Delta\sigma}{\delta}\right)_2 \cos(2\Psi_2) (I_2 - \tau_2 I_1) \quad (28)$$

$$U \approx - \left(\frac{\Delta\sigma}{\delta}\right)_3 \sin(2\Psi_3) [I_1 + I_3 - \tau_3(I_1 + I_2)] - \left(\frac{\Delta\sigma}{\delta}\right)_2 \sin(2\Psi_2) (I_2 - \tau_2 I_1) \quad (29)$$

$$V \approx \sin(2\Psi_2 - 2\Psi_1) \left[\left(\frac{\Delta\epsilon}{\delta}\right)_2 \left(\frac{\Delta\sigma}{\delta}\right)_1 \tau_2 I_1 + \left(\frac{\Delta\epsilon}{\delta}\right)_3 \left(\frac{\Delta\sigma}{\delta}\right)_2 \tau_3 I_2 \right]. \quad (30)$$

The direction and magnitude of linear polarization at selected positions are shown in Figure 5 for a stratified disk model with parameters given in Table 1, viewed at inclination $\theta_i = 45^\circ$. Figure 5c,d show the linear and circular polarization as a function of azimuthal angle (in the disk plane) for

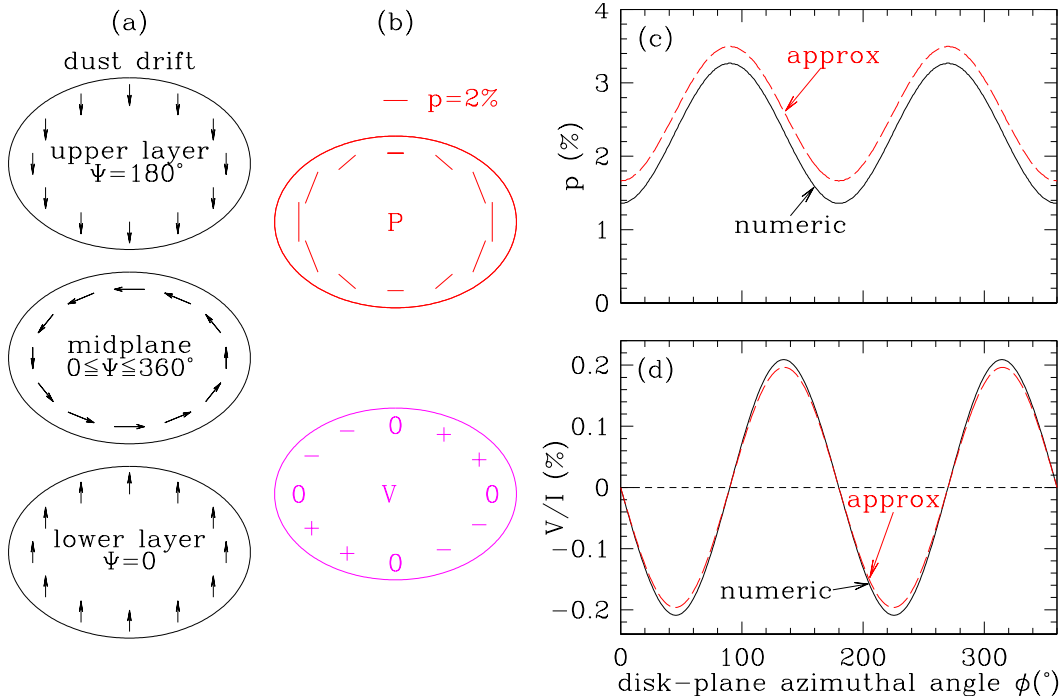


Figure 5. (a) Grain drift directions in a stratified disk (see text). (b) Upper figure: the direction of linear polarization if the grains are aligned by $\mathbf{v}_{\text{drift}}$, with parameters in Table 1. The length of the line segment is proportional to the fractional polarization, with the scale bar showing 2% fractional polarization. Lower figure: quadrupolar pattern for circular polarization V for the example discussed in the text. (c) Fractional linear polarization $p = (Q^2 + U^2)^{1/2}/I$ for stratified disk model (see Table 1), viewed at inclination $\theta_i = 45^\circ$ (see text), as a function of azimuthal angle in the disk plane. $\phi = 0$ is along the minor axis. (d) Circular polarization V/I for this model.

this model. In addition to accurate results from numerical integration, the results from the analytic approximation (Eqs. 28–30) are also plotted. The analytic approximation is seen to provide fair accuracy, even though $\tau_2 = 0.2$ is not small.

The circular polarization V/I is quite accurate, but in Figure 5(c), the analytic approximation slightly overestimates the linear polarization fraction. However, the analytic approximations were developed for $\tau \ll 1$, and here the total optical depth $\tau_1 + \tau_2 + \tau_3 = 0.3$ is not small.

For this model, the linear polarization varies from 1.4% to 3.2% around the disk, with average value $\sim 2.5\%$. The linear polarization tends to be close to the azimuthal direction, with largest values on the major axis, and smallest values along the minor axis of inclined disk (see Figure 5).

The predicted circular polarization $|V|/I$ is small but perhaps detectable, with V/I varying from positive to negative from one quadrant to another (see Figure 5), with maxima $|V|/I \approx 0.2\%$ (see Figure 5(d)).

Stephens et al. (2017) mapped V over the HL Tau disk at 3.3 mm, 1.3 mm, and $870\mu\text{m}$. The 3.3 mm V map does not appear to show any statistically significant detection, with upper limits $|V/I| \lesssim 1\%$. At 1.3 mm and $870\mu\text{m}$ the NW side of the major axis may have $V/I \approx -1\%$, but whether this is real rather than an instrumental artifact remains unclear. In any event, the likely importance of scattering at these shorter wavelengths will complicate interpretation.

6. DISCUSSION

For typical molecular clouds we conclude that the circular polarization will be undetectably small at the far-infrared and submm wavelengths where the clouds radiate strongly. Probing the magnetic field structure in such clouds using circular polarization is feasible only at shorter infrared wavelengths where the extinction is appreciable, using embedded infrared sources (stars, protostars, or PDRs).

The thermal dust emission from so-called IR dark clouds (IRDCs) in the inner Galaxy – such as the “Brick” – can show appreciable levels of linear polarization, demonstrating both that there is appreciable grain alignment *and* that the magnetic field structure in the cloud, while showing evidence of rotation, is relatively coherent. IRDCs have large enough column densities that the resulting circular polarization may reach detectable levels. For one position on the Brick and plausible assumptions concerning the field, we estimate a circular polarization $|V/I| \approx 0.025\%$ at 850 GHz. If the circular polarization can be detected and mapped in IRDCs, it would provide constraints on the 3-dimensional magnetic field structure. Unfortunately, the predicted V/I is small, especially at longer wavelengths (we expect $V/I \propto \lambda^{-1.1}$), and detection will be challenging.

Protoplanetary disks may offer the best opportunity to measure circular polarization at submm wavelengths. If there are significant changes in the direction of grain alignment between the dust near the midplane and dust well above and below the midplane, linear dichroism and birefringence will produce circular polarization. Alignment processes in protoplanetary disks remain uncertain, but we suggest that grain drift may cause the grains near the midplane to be aligned with long axes preferentially in the azimuthal direction, while grains above and below the midplane may be aligned with long axes tending to be in the vertical direction (normal to the disk). If the grains are small enough that scattering can be neglected, we calculate the linear and circular polarization that would be expected for such a model. A characteristic quadrupole pattern of circular polarization is predicted for this kind of grain alignment (see Figure 5). Eq. (30) can be used to estimate the circular polarization at wavelengths $\lambda \gtrsim 100\mu\text{m}$ where thermal emission is strong and the grains may be approximated by the Rayleigh limit.

We present a simple example to show the linear and circular polarization that might be present in protoplanetary disks, such as the disk around HL Tau. This example is not being put forward as a realistic model for HL Tau, but simply to illustrate the possible circular polarization from dust aligned by streaming in a stratified disk. If observed, this would help clarify the physical processes responsible for grain alignment in protoplanetary disks. Absence of this circular polarization would indicate that the preferred direction for grain alignment in high-altitude regions is the same as the

preferred direction near the midplane, or else that grain alignment occurs only in the midplane, or only in the upper layers.

If circular polarization is detected and mapped in a protoplanetary disk, interpretation will require radiative transfer models that include the birefringence and dichroism discussed here as well as the circular polarization produced by scattering of linearly polarized radiation. Models will be sensitive to the spatial distribution of the dust, and also to the sizes and scattering properties of the solid particles. Maps of V/I at multiple frequencies would strongly constrain protoplanetary disk models.

7. SUMMARY

1. We present the transfer equations for the Stokes parameters, including the effects of thermal emission. Once the properties of the medium are specified, these equations can easily be integrated numerically. For small optical depths, analytic solutions are given for clouds with a uniform twist to the magnetic field, and for stratified clouds with uniform alignment within individual strata.
2. Using the “astrodust” grain model (Draine & Hensley 2021b) we calculate the relevant optical properties of dust grains for producing linear and circular polarization in the far-infrared and submm. By adjusting the assumed degree of dust alignment f_{align} , these dust properties may approximate the properties of dust in protoplanetary disks, at wavelengths where scattering can be neglected.
3. At submm wavelengths, the “phase shift” cross section C_{pha} tends to be much larger than the absorption cross section C_{abs} . We estimate $C_{\text{pha}}/C_{\text{abs}} \approx 24(\lambda/\text{mm})^{0.7}$.
4. The far-IR emission from dust in diffuse clouds, and in normal molecular clouds, will have very low levels of circular polarization, below current and foreseen sensitivities.
5. If the magnetic field in IRDCs has a significant systematic twist, the emission from IRDCs – such as the “Brick” – may have $V/I \approx 0.025\%(\lambda/350\mu\text{m})^{-1.1}$
6. If dust grains in protoplanetary disks are aligned in different directions in different strata, the resulting submm emission may be circularly polarized with peak $V/I \approx 0.2\%(\lambda/350\mu\text{m})^{-1.1}$ for one simple example with parameters suggested by HL Tau. Measuring the circular polarization can constrain the mechanisms responsible for grain alignment in protoplanetary disks.

This work was supported in part by NSF grant AST-1908123. I thank Yilun Guan, Chat Hull and Joseph Weingartner for helpful discussions, Robert Lupton for availability of the SM package. I thank the anonymous referee for helpful suggestions that improved this paper.

REFERENCES

- | | |
|--|--|
| <p>Aitken, D. K., Hough, J. H., & Chrysostomou, A. 2006, <i>MNRAS</i>, 366, 491, doi: 10.1111/j.1365-2966.2005.09873.x</p> <p>Andersson, B.-G., Lazarian, A., & Vaillancourt, J. E. 2015, <i>ARA&A</i>, 53, 501, doi: 10.1146/annurev-astro-082214-122414</p> <p>Andrews, S. M., Huang, J., Pérez, L. M., et al. 2018, <i>ApJL</i>, 869, L41, doi: 10.3847/2041-8213/aaf741</p> <p>Beckwith, S. V. W., & Sargent, A. I. 1991, <i>ApJ</i>, 381, 250, doi: 10.1086/170646</p> | <p>Bohren, C. F., & Huffman, D. R. 1983, <i>Absorption and Scattering of Light by Small Particles</i> (New York: Wiley)</p> <p>Carey, S. J., Clark, F. O., Egan, M. P., et al. 1998, <i>ApJ</i>, 508, 721, doi: 10.1086/306438</p> <p>Chuss, D. T., Andersson, B. G., Bally, J., et al. 2019, <i>ApJ</i>, 872, 187, doi: 10.3847/1538-4357/aafd37</p> <p>Das, I., & Weingartner, J. C. 2016, <i>MNRAS</i>, 457, 1958, doi: 10.1093/mnras/stw146</p> |
|--|--|

- Davis, L. J., & Greenstein, J. L. 1951, *ApJ*, 114, 206, doi: [10.1086/145464](https://doi.org/10.1086/145464)
- Dotson, J. L., Vaillancourt, J. E., Kirby, L., et al. 2010, *ApJS*, 186, 406, doi: [10.1088/0067-0049/186/2/406](https://doi.org/10.1088/0067-0049/186/2/406)
- Draine, B. T. 2006, *ApJ*, 636, 1114, doi: [10.1086/498130](https://doi.org/10.1086/498130)
- Draine, B. T., & Hensley, B. S. 2021a, *ApJ*, 919, 65, doi: [10.3847/1538-4357/ac0050](https://doi.org/10.3847/1538-4357/ac0050)
- . 2021b, *ApJ*, 909, 94, doi: [10.3847/1538-4357/abd6c6](https://doi.org/10.3847/1538-4357/abd6c6)
- Draine, B. T., & Lee, H. M. 1984, *ApJ*, 285, 89, doi: [10.1086/162480](https://doi.org/10.1086/162480)
- Draine, B. T., & Weingartner, J. C. 1996, *ApJ*, 470, 551, doi: [10.1086/177887](https://doi.org/10.1086/177887)
- . 1997, *ApJ*, 480, 633, doi: [10.1086/304008](https://doi.org/10.1086/304008)
- Dyck, H. M., & Lonsdale, C. J. 1981, in *Infrared Astronomy*, ed. C. G. Wynn-Williams & D. P. Cruikshank, Vol. 96, 223–233
- Fissel, L. M., Ade, P. A. R., Angilè, F. E., et al. 2016, *ApJ*, 824, 134, doi: [10.3847/0004-637X/824/2/134](https://doi.org/10.3847/0004-637X/824/2/134)
- Fukushima, H., Yajima, H., & Umemura, M. 2020, *MNRAS*, 496, 2762, doi: [10.1093/mnras/staa1718](https://doi.org/10.1093/mnras/staa1718)
- Gold, T. 1952, *MNRAS*, 112, 215, doi: [10.1093/mnras/112.2.215](https://doi.org/10.1093/mnras/112.2.215)
- Guan, Y., Clark, S. E., Hensley, B. S., et al. 2021, *ApJ*, 920, 6, doi: [10.3847/1538-4357/ac133f](https://doi.org/10.3847/1538-4357/ac133f)
- Hall, J. S. 1949, *Science*, 109, 166, doi: [10.1126/science.109.2825.166](https://doi.org/10.1126/science.109.2825.166)
- Hamaker, J. P., & Bregman, J. D. 1996, *A&AS*, 117, 161
- Hensley, B. S., & Draine, B. T. 2021, *ApJ*, 906, 73, doi: [10.3847/1538-4357/abc8f1](https://doi.org/10.3847/1538-4357/abc8f1)
- Hiltner, W. A. 1949, *Nature*, 163, 283, doi: [10.1038/163283a0](https://doi.org/10.1038/163283a0)
- Hoang, T., Cho, J., & Lazarian, A. 2018, *ApJ*, 852, 129, doi: [10.3847/1538-4357/aa9edc](https://doi.org/10.3847/1538-4357/aa9edc)
- Kataoka, A., Okuzumi, S., & Tazaki, R. 2019, *ApJL*, 874, L6, doi: [10.3847/2041-8213/ab0c9a](https://doi.org/10.3847/2041-8213/ab0c9a)
- Kataoka, A., Tsukagoshi, T., Pohl, A., et al. 2017, *ApJL*, 844, L5, doi: [10.3847/2041-8213/aa7e33](https://doi.org/10.3847/2041-8213/aa7e33)
- Kataoka, A., Muto, T., Momose, M., et al. 2015, *ApJ*, 809, 78, doi: [10.1088/0004-637X/809/1/78](https://doi.org/10.1088/0004-637X/809/1/78)
- Kemp, J. C. 1972, *ApJL*, 175, L35, doi: [10.1086/180979](https://doi.org/10.1086/180979)
- Kemp, J. C., & Wolstencroft, R. D. 1972, *ApJL*, 176, L115, doi: [10.1086/181036](https://doi.org/10.1086/181036)
- Kwon, J., Tamura, M., Hough, J. H., Nagata, T., & Kusakabe, N. 2016, *AJ*, 152, 67, doi: [10.3847/0004-6256/152/3/67](https://doi.org/10.3847/0004-6256/152/3/67)
- Kwon, J., Tamura, M., Hough, J. H., et al. 2014, *ApJL*, 795, L16, doi: [10.1088/2041-8205/795/1/L16](https://doi.org/10.1088/2041-8205/795/1/L16)
- Kwon, J., Nakagawa, T., Tamura, M., et al. 2018, *AJ*, 156, 1, doi: [10.3847/1538-3881/aac389](https://doi.org/10.3847/1538-3881/aac389)
- Lazarian, A. 1994, *MNRAS*, 268, 713, doi: [10.1093/mnras/268.3.713](https://doi.org/10.1093/mnras/268.3.713)
- Lazarian, A., & Hoang, T. 2007a, *MNRAS*, 378, 910, doi: [10.1111/j.1365-2966.2007.11817.x](https://doi.org/10.1111/j.1365-2966.2007.11817.x)
- . 2007b, *ApJL*, 669, L77, doi: [10.1086/523849](https://doi.org/10.1086/523849)
- Lee, C.-F., Li, Z.-Y., Yang, H., et al. 2021, *ApJ*, 910, 75, doi: [10.3847/1538-4357/abe53a](https://doi.org/10.3847/1538-4357/abe53a)
- Lee, H. M., & Draine, B. T. 1985, *ApJ*, 290, 211, doi: [10.1086/162974](https://doi.org/10.1086/162974)
- Longmore, S. N., Rathborne, J., Bastian, N., et al. 2012, *ApJ*, 746, 117, doi: [10.1088/0004-637X/746/2/117](https://doi.org/10.1088/0004-637X/746/2/117)
- Lonsdale, C. J., Dyck, H. M., Capps, R. W., & Wolstencroft, R. D. 1980, *ApJL*, 238, L31, doi: [10.1086/183251](https://doi.org/10.1086/183251)
- Marsh, K. A., Ragan, S. E., Whitworth, A. P., & Clark, P. C. 2016, *MNRAS*, 461, L16, doi: [10.1093/mnras/461.1/L16](https://doi.org/10.1093/mnras/461.1/L16)
- Martin, P. G. 1972, *MNRAS*, 159, 179, doi: [10.1093/mnras/159.2.179](https://doi.org/10.1093/mnras/159.2.179)
- . 1974, *ApJ*, 187, 461, doi: [10.1086/152655](https://doi.org/10.1086/152655)
- Martin, P. G., & Angel, J. R. P. 1976, *ApJ*, 207, 126, doi: [10.1086/154476](https://doi.org/10.1086/154476)
- Martin, P. G., & Campbell, B. 1976, *ApJ*, 208, 727, doi: [10.1086/154656](https://doi.org/10.1086/154656)
- Martin, P. G., Illing, R., & Angel, J. R. P. 1972, *MNRAS*, 159, 191, doi: [10.1093/mnras/159.2.191](https://doi.org/10.1093/mnras/159.2.191)
- Molinari, S., Schisano, E., Elia, D., et al. 2016, *A&A*, 591, A149, doi: [10.1051/0004-6361/201526380](https://doi.org/10.1051/0004-6361/201526380)
- Mori, T., & Kataoka, A. 2021, *ApJ*, 908, 153, doi: [10.3847/1538-4357/abd08a](https://doi.org/10.3847/1538-4357/abd08a)
- Natta, A., & Testi, L. 2004, in *Astr. Soc. Pac. Conf. Ser. 323, Star Formation in the Interstellar Medium: In Honor of David Hollenbach*, ed. D. Johnstone, F. C. Adams, D. N. C. Lin, D. A. Neufeld, & E. C. Ostriker, 279
- Okuzumi, S., & Tazaki, R. 2019, *ApJ*, 878, 132, doi: [10.3847/1538-4357/ab204d](https://doi.org/10.3847/1538-4357/ab204d)

- Planck Collaboration, Ade, P. A. R., Aghanim, N., et al. 2015a, *A&A*, 576, A104, doi: [10.1051/0004-6361/201424082](https://doi.org/10.1051/0004-6361/201424082)
- . 2015b, *A&A*, 576, A106, doi: [10.1051/0004-6361/201424087](https://doi.org/10.1051/0004-6361/201424087)
- Planck Collaboration, Aghanim, N., Akrami, Y., et al. 2020, *A&A*, 641, A12, doi: [10.1051/0004-6361/201833885](https://doi.org/10.1051/0004-6361/201833885)
- Purcell, E. M. 1969, *Physica*, 41, 100, doi: [10.1016/0031-8914\(69\)90243-2](https://doi.org/10.1016/0031-8914(69)90243-2)
- Reissl, S., Wolf, S., & Brauer, R. 2016, *A&A*, 593, A87, doi: [10.1051/0004-6361/201424930](https://doi.org/10.1051/0004-6361/201424930)
- Serkowski, K. 1962, *Advances in Astronomy and Astrophysics*, 1, 289, doi: [10.1016/B978-1-4831-9919-1.50009-1](https://doi.org/10.1016/B978-1-4831-9919-1.50009-1)
- Serkowski, K., & Rieke, G. H. 1973, *ApJL*, 183, L103, doi: [10.1086/181263](https://doi.org/10.1086/181263)
- Stephens, I. W., Yang, H., Li, Z.-Y., et al. 2017, *ApJ*, 851, 55, doi: [10.3847/1538-4357/aa998b](https://doi.org/10.3847/1538-4357/aa998b)
- Takeuchi, T., & Lin, D. N. C. 2002, *ApJ*, 581, 1344, doi: [10.1086/344437](https://doi.org/10.1086/344437)
- van de Hulst, H. C. 1957, *Light Scattering by Small Particles* (New York: John Wiley & Sons)
- Walker, D. L., Longmore, S. N., Bally, J., et al. 2021, *MNRAS*, 503, 77, doi: [10.1093/mnras/stab415](https://doi.org/10.1093/mnras/stab415)
- Weingartner, J. C., & Draine, B. T. 2003, *ApJ*, 589, 289, doi: [10.1086/374597](https://doi.org/10.1086/374597)
- Yang, H. 2021, *ApJ*, 911, 125, doi: [10.3847/1538-4357/abebde](https://doi.org/10.3847/1538-4357/abebde)

APPENDIX

A. UNIFORM TWIST

Assume a single dust temperature T_d . Define $d\tau' \equiv \delta dz$. Suppose Ψ varies linearly with τ , with total twist $\Delta\Psi$:

$$\Psi(\tau') = \Psi_0 + \alpha\tau' \quad , \quad \alpha = \frac{\Delta\Psi}{\tau} \quad . \quad (\text{A1})$$

Assuming $\mathbf{S} = (0, 0, 0, 0)$ for $\tau = 0$, and integrating Eq. (10) while retaining only low-order terms in τ , we obtain:

$$I \approx B(T_d)\tau \left\{ 1 - \frac{1}{2}\tau - \left(\frac{\Delta\sigma}{\delta}\right)^2 \tau \frac{[1 - \cos(2\Delta\Psi)]}{4(\Delta\Psi)^2} \right\} \quad (\text{A2})$$

$$Q \approx -\left(\frac{\Delta\sigma}{\delta}\right) B(T_d)\tau (1 - \tau) \frac{[\sin(2\Psi) - \sin(2\Psi_0)]}{2\Delta\Psi} \quad (\text{A3})$$

$$U \approx -\left(\frac{\Delta\sigma}{\delta}\right) B(T_d)\tau (1 - \tau) \frac{[\cos(2\Psi_0) - \cos(2\Psi)]}{2\Delta\Psi} \quad (\text{A4})$$

$$V \approx \left(\frac{\Delta\sigma}{\delta}\right) \left(\frac{\Delta\epsilon}{\delta}\right) \frac{B(T_d)\tau^2}{2\Delta\Psi} \left\{ 1 - \frac{1}{2}\tau + \frac{\tau}{(2\Delta\Psi)^2} [\cos(2\Delta\Psi) - 1] - \frac{(1 - \tau)}{2\Delta\Psi} \sin(2\Delta\Psi) \right\} \quad (\text{A5})$$

$$p \equiv \frac{(Q^2 + U^2)^{1/2}}{I} \approx \frac{1}{\Delta\Psi} \left(\frac{\delta\sigma}{\delta}\right) \frac{(1 - \tau) [1 - \cos(2\Delta\Psi)]^{1/2}}{1 - \frac{1}{2}\tau - \tau \left(\frac{\Delta\sigma}{\delta}\right)^2 \frac{1 - \cos(2\Delta\Psi)}{4(\Delta\Psi)^2}} \quad . \quad (\text{A6})$$

These results are valid for $\tau \ll 1$, and general twist angle $\Delta\Psi$.

B. A TWO ZONE MODEL

Suppose that $\Psi = \Psi_1$ for $0 < \tau < \tau_1$ and $\Psi = \Psi_1 + \Delta\Psi(\tau - \tau_1)/\tau_2$ for $\tau_1 < \tau < \tau_1 + \tau_2$. Let $T_d = T_{d1}$ for $0 < \tau < \tau_1$, and $T_d = T_{d2}$ for $\tau_1 < \tau < \tau_1 + \tau_2$. Define

$$A \equiv \frac{\Delta\sigma}{\delta} [I_1 - B(T_{d2})] \quad . \quad (\text{B7})$$

Assuming $\mathbf{S} = (0, 0, 0, 0)$ for $\tau = 0$, integrating Eq. (10), retaining only low-order terms in τ , we obtain $\mathbf{S}_1 = (I_1, Q_1, U_1, V_1)$ at $\tau = \tau_1$, and $\mathbf{S}_2 = (I_2, Q_2, U_2, V_2)$ at $\tau = \tau_1 + \tau_2$:

$$I_1 = B(T_{d1})(1 - e^{-\tau_1}) \quad (\text{B8})$$

$$Q_1 = -\left(\frac{\Delta\sigma}{\delta}\right)_1 \cos(2\Psi_1) I_1 \quad (\text{B9})$$

$$U_1 = -\left(\frac{\Delta\sigma}{\delta}\right)_1 \sin(2\Psi_1) I_1 \quad (\text{B10})$$

$$V_1 = 0 \quad (\text{B11})$$

$$I_2 \approx I_1 e^{-\tau_2} + B(T_{d2})(1 - e^{-\tau_2}) \quad (\text{B12})$$

$$Q_2 \approx Q_1(1 - \tau_2) + A\tau_2(1 - \tau_2) \frac{\sin(2\Psi_2) - \sin(2\Psi_1)}{2\Delta\Psi} \quad (\text{B13})$$

$$U_2 \approx U_1(1 - \tau_2) + A\tau_2(1 - \tau_2) \frac{\cos(2\Psi_1) - \sin(2\Psi_2)}{2\Delta\Psi} \quad (\text{B14})$$

$$\begin{aligned}
V_2 \approx & \left(\frac{\Delta\epsilon}{\delta} \right)_2 Q_1 \left[\tau_2 \frac{\cos 2\Psi_2 - \cos 2\Psi_1}{2\Delta\Psi} - \tau_2^2 \frac{\sin 2\Psi_2 - \sin 2\Psi_1 - 2\Delta\Psi \cos 2\Psi_2}{2\Delta\Psi} \right] \\
& + \left(\frac{\Delta\epsilon}{\delta} \right)_2 U_1 \left[\tau_2 \frac{\sin 2\Psi_2 - \sin 2\Psi_1}{2\Delta\Psi} - \tau_2^2 \frac{\cos 2\Psi_2 - \cos 2\Psi_1 - 2\Delta\Psi \sin 2\Psi_2}{2\Delta\Psi} \right] \\
& - \left(\frac{\Delta\epsilon}{\delta} \right)_2 A \frac{\tau_2}{2\Delta\Psi} \left[\tau_2 - \frac{1}{2} \tau_2^2 \right] + \left(\frac{\Delta\epsilon}{\delta} \right)_2 A \left(\frac{\tau_2}{2\Delta\Psi} \right)^2 \sin 2\Delta\Psi \\
& + \left(\frac{\Delta\epsilon}{\delta} \right)_2 A \left(\frac{\tau_2}{2\Delta\Psi} \right)^3 [1 - \cos 2\Delta\Psi - 2\Delta\Psi \sin 2\Delta\Psi] + O(\tau_2^4) \quad .
\end{aligned} \tag{B15}$$

C. THREE ZONE MODEL

Suppose the dust is located in three zones, with dust temperatures T_{d1} , T_{d2} , and T_{d3} . The aligned dust grains have $\Psi = \Psi_1$ for $0 < \tau < \tau_1$, $\Psi = \Psi_2$ for $\tau_1 < \tau < \tau_1 + \tau_2$, and $\Psi = \Psi_3$ for $\tau_1 + \tau_2 < \tau < \tau_1 + \tau_2 + \tau_3$. Suppose all $\tau_j \ll 1$.

Define

$$I_1 \equiv B(T_{d1}) [1 - e^{-\tau_1}] e^{-\tau_2 - \tau_3} \approx B(T_{d1}) \tau_1 \left[1 - \frac{1}{2} \tau_1 \right] e^{-\tau_2 - \tau_3} \tag{C16}$$

$$I_2 \equiv B(T_{d2}) [1 - e^{-\tau_2}] e^{-\tau_3} \approx B(T_{d2}) \tau_2 \left[1 - \frac{1}{2} \tau_2 \right] e^{-\tau_3} \tag{C17}$$

$$I_3 \equiv B(T_{d3}) [1 - e^{-\tau_3}] \approx B(T_{d3}) \tau_3 \left[1 - \frac{1}{2} \tau_3 \right] \tag{C18}$$

If $\mathbf{S} = (0, 0, 0, 0)$ for $\tau = 0$, then the radiation emerging from layer 3 has

$$I \approx I_1 + I_2 + I_3 \tag{C19}$$

$$Q \approx - \left(\frac{\Delta\sigma}{\delta} \right)_1 \cos(2\Psi_1) I_1 - \left(\frac{\Delta\sigma}{\delta} \right)_2 \cos(2\Psi_2) [I_2 - \tau_2 I_1] - \left(\frac{\Delta\sigma}{\delta} \right)_3 \cos(2\Psi_3) [I_3 - \tau_3 (I_1 + I_2)] \tag{C20}$$

$$U \approx - \left(\frac{\Delta\sigma}{\delta} \right)_1 \sin(2\Psi_1) I_1 - \left(\frac{\Delta\sigma}{\delta} \right)_2 \sin(2\Psi_2) [I_2 - \tau_2 I_1] - \left(\frac{\Delta\sigma}{\delta} \right)_3 \sin(2\Psi_3) [I_3 - \tau_3 (I_1 + I_2)] \tag{C21}$$

$$\begin{aligned}
V \approx & \left(\frac{\Delta\epsilon}{\delta} \right)_2 \left(\frac{\Delta\sigma}{\delta} \right)_1 \sin(2\Psi_2 - 2\Psi_1) \tau_2 I_1 + \left(\frac{\Delta\epsilon}{\delta} \right)_3 \left(\frac{\Delta\sigma}{\delta} \right)_1 \sin(2\Psi_3 - 2\Psi_1) \tau_3 I_1 \\
& + \left(\frac{\Delta\epsilon}{\delta} \right)_3 \left(\frac{\Delta\sigma}{\delta} \right)_2 \sin(2\Psi_3 - 2\Psi_2) \tau_3 I_2 \quad .
\end{aligned} \tag{C22}$$